For the published article, please see:
https://doi.org/10.1016/j.isatra.2013.08.006

Optimised Sensor Selection for Control and Fault Tolerance of Electromagnetic Suspension Systems: a Robust Loop Shaping Approach

Abstract

This paper presents a systematic design framework for selecting the sensors in an optimised manner, simultaneously satisfying a set of given complex system control requirements, i.e. optimum and robust performance as well as fault tolerant control for high integrity systems. It is worth noting that optimum sensor selection in control system design is often a non-trivial task. Among all candidate sensor sets, the algorithm explores and separately optimises system performance with all the feasible sensor sets in order to identify fallback options under single or multiple sensor faults. The proposed approach combines modern robust control design, fault tolerant control, multiobjective optimisation and Monte Carlo techniques. Without loss of generality, it's efficacy is tested on an electromagnetic suspension system via appropriate realistic simulations.

Keywords: Optimised sensor selection, Robust control, Fault tolerant control, Magnetic levitation, Multi-objective optimisation, Electromagnetic Suspension

1. Introduction

Optimum sensor selection in practical control system design can be complex process especially if the selection is done with respect to a number of properties in order to achieve robust optimum performance and reliability properties.

A typical closed-loop control system is shown in Fig. 1. Typically, a system to be controlled has a number of candidate control inputs (actuators) and outputs (sensors) that could be used to control it by proper controller design using one of the existing modern control methods. Moreover the system suffers from input disturbances and uncertainties or model inaccuracies. Additionally, faults highly

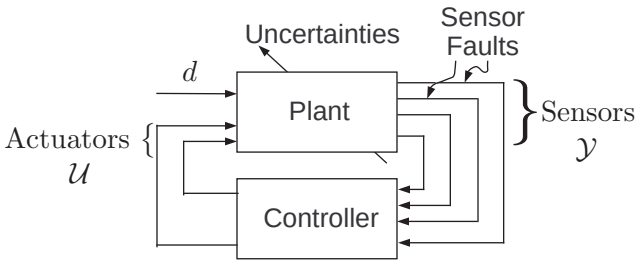

Figure 1: A typical closed-loop control system.

affect the closed-loop performance of a control system. Particularly, actuator and sensor faults can

cause performance degradation or even instability. This problem has been extensively considered by the scientific community the last years. Some typical work with applications to industrial systems includes [1], [2], [3] and [4].

The problem of sensor/actuator selection has been addressed before in the literature [5] but none of the methods consider simultaneous satisfaction of the aforementioned properties except in [6] where the authors have consider both optimum performance and sensor fault tolerance using **L**inear **Q**uadratic **G**aussian (LQG) control. Therefore the problem is to find the 'best' set of sensors, $\mathcal{Y}_o$, subject to the aforementioned control properties i.e. optimum performance, robustness, fault tolerance and minimum number of sensors.

The novelty in this paper relies in the fact that optimum robust performance with sensor fault tolerance is achieved by combining robust control methods, **F**ault **T**olerant **C**ontrol (FTC), **M**ulti-**O**bjective **OP**timisation (MOOP) and **M**onte **C**arlo (MC) method as illustrated in Fig. 2.

Robust control design in a practical control system has a vital role because real systems have

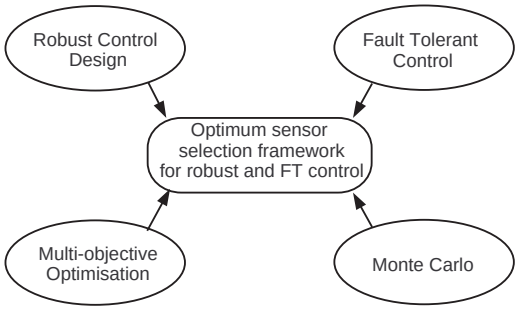

Figure 2: The simplified diagram of the proposed framework for optimum sensor selection with robust control and fault tolerance.

uncertainties, disturbance inputs and other effects that affects the nominal performance of the closed-loop control system. In that context robust control theory has been developed the last years including $\mathcal{H}_\infty$ robust control control methods [7]. Among the existing robust control methods the $\mathcal{H}_\infty$ **L**oop **S**haping **D**esign **P**rocedure (LSDP) is merged into the framework for the design of robust nominal controller [8].

Control system design for safety-critical systems [9, 10] is vital for the integrity of such systems when sub-systems faults occur. Therefore the scientific community developed an area where the faults can be accommodated. Fault tolerant control systems are divided into two categories, the **A**ctive FTC (AFTC) and the **P**assive FTC (PFTC) systems. In this work, the AFTC concept is introduced in order to accommodate multiple sensor faults [11, 12, 13].

Multiobjective constrained optimisation using heuristic approaches is very popular and has gained a lot of intention the last years [14, 15]. Among the heuristic methods, **G**enetic **A**lgorithms (GA) are favour in control optimisation [16, 17, 18]. Since the beginning of GAs by Goldberg (1989) [19] many versions of GAs have been published all summarised in [20] with the latest version called **D**ynamical **M**ultiobjective **E**volutionary **A**lgorithm (DMOEA) been described in [21]. In this paper the **N**on-dominated **S**orting **G**enetic **A**lgorithm II (NSGAII) [22] is used for the optimisation part of the framework and shows to be very strong optimisation tool in sensor selection for control design.

Monte Carlo method has gained a lot of attention after the initial introduction by N. Metropo-

lis (1949,1987) [23, 24]. Until today many methods have been introduced for random generation of numbers with this method [25, 26]. Moreover the MC method can be used in control systems to assess the robustness in a probabilistic way [27]. In this paper the robustness against model parametric uncertainties is assessed using a combination of the MC and constraint handling functions as used in MOOP. Particularly, the MC is used to produce a number of models for the uncertainties and those are tested in closed-loop simulations using the nominal controller.

The proposed framework is assessed on an **E**lectro-**M**agnetic **S**uspension (EMS) system. The EMS systems are being used on the **MAG**netic **LEV**itated (MAGLEV) trains that have a number of advantages against the conventional wheel-on-rail trains [28]. As indicated in [29] the EMS is **N**on-**L**inear (NL), safety-critical and inherently unstable system with non-trial requirements. Such system can easily serve as a good example for testing the efficacy of the proposed optimum sensor selection framework.

Summarizing, the novelty in this article relies on the fact that $\mathcal{H}_\infty$ Robust Control, FTC, MC method and optimised tuning via GAs concepts are combined to form a systematic framework in an attempt to simplify the selection of the best sensor set defined as, $\mathcal{Y}_o$, for the EMS system subject to optimum closed-loop performance and ensuring integrity and robustness of the system under possible sensor faults. In this context, the algorithm explores and separately optimises the performance of the EMS using all feasible sensor sets in order to identify fallback options under single or multiple sensor faults, i.e. instants of one or multiple sensors failing stability constraints but with optimum performance maintained by controller reconfiguration using the remaining healthy sensors.

The rest of the paper is separated into six sections: Section 2 explains the problem under consideration and describes the details of the proposed algorithm that leads to the optimum sensor selection for the control system design. The next Section 3 describes the rigorous modelling issues of the EMS system along with the disturbance inputs and multiple control objectives and constraints requirements. In Section 4 the multiobjective constraint optimisation concept as used in the algorithm is given emphasizing its usefulness and importance. Further Section describes the sensor fault tolerance concept for the EMS system with the robustness assessment of the optimally tuned controller using the Monte Carlo method in combination with constraint handling technique as used in previous section. In Section 6 data analysis is done from the realistic simulations done from the proposed framework. Finally, the conclusions of this work are given in the last Section 7.

2. The problem statement and description of the proposed framework

2.1. Problem statement

The plant shown in Fig. 1 has a set of control inputs (actuators) $\mathcal{U} = \{u_1, u_2, \dots u_{n_u}\}$, where n_u is the total number of actuators, a set of input disturbances $\mathcal{D} = \{d_1, d_2, \dots d_{n_d}\}$, where n_d is the total number of input disturbances, and a set of possible outputs (sensors), $\{\mathcal{Y} = y_1, y_2, \dots y_{n_s}\}$, where n_s is the total number of sensors, and a set of sensor sub-sets of $\mathcal{Y}$, $\mathbb{Y} = \{\mathcal{Y}_1, \mathcal{Y}_2 \dots \mathcal{Y}_{N_{ss}}\}$ to choose from, where N_{ss} is the total number of sensor sub-sets in $\mathbb{Y}$. The formal problem is defined as to determine the set of sensors, $\mathcal{Y}_o$, in $\mathbb{Y}$ (i.e. select $\mathcal{Y}_o \subset \mathbb{Y}(i)$), for which the system

1. satisfies a set of closed-loop performance criteria,
2. satisfies a set of fault tolerance criteria,
3. the sensor set has minimum redundancy i.e. the number of elements in $\mathcal{Y}_o$ is minimal,

4. has sufficient robustness against parametric uncertainties and
5. has low cost (although this property is not considered in the paper, its part of this problem and left for future work).

The following section gives a rigorous description of the proposed algorithm which attempts to solve this problem.

2.2. The proposed framework

The proposed framework can be summarised in the flow chart of Fig. 3. The particular points include the use of $\mathcal{H}_\infty$ loop-shaping design and the heuristic optimisation (evolutionary algorithms) method for tuning the controller subject to strict requirements (objectives and constraints) for each feasible sensor set of the EMS system. Prior to running the algorithm (initialization phase), some parameters are assigned including:

- *Formulate the model of the system*: Prior to algorithm execution formulate the model of the system to be examined. i.e. non-linearities, uncertainties, linearization etc.
- *Generate the sensor sets*: A set, $\mathbb{Y}$, which contains all sensor sets is generated at this stage.
- *Define the control objective functions* (ϕ_i) *and constraints* (f_h, f_s): Usually, in a system's optimisation the control objectives are conflicting to each other therefore a trade-off exists between them. Also there is a number of control constraints that have to be satisfied in order for the system to have proper control properties. Both can be time of frequency related characteristics and will effectively define the optimum performance of the closed-loop.
- *Enter the performance weights*: Since the LSDP is used for the design of the controller the structure of the **P**erformance **W**eights (PW) has to be decided. This will effectively have one PW for each measurement for the loop-shaping and it has to be optimally tuned for each feasible sensor set using the NSGAII.
- *Robustness assessment parameters*: Each sensor set is tested for robustness against parametric uncertainties using MC and the **W**eighted **O**verall **C**onstraint **V**iolation **F**unction (WOCVF). Some parameters have to be assigned for the robustness assessment like the number of uncertain samples to be tested, N_{mc} and the **C**onstraint **V**iolation **W**eights (CVWs), w_i with the latter been rigorously described in Section 4.
- *Enter the optimisation parameters*: As it has been mentioned the NSGAII will be used for the optimisation part of the proposed framework. As all GAs this also requires some parameter assignment which effectively affects the successful recovery of the optimum Pareto front between the objective functions. This parameter assignment includes: The mutation probability p_m, crossover probability p_c, population number N_p, maximum generation number N_g, penalty parameters, number of variables n_u and the search space for each variable.
- *Enter the controller selection criteria*: After the optimisation completion for each sensor set there is a number of controllers that result to a closed-loop performance equal to the number of population of the NSGAII. Among those the best one which suites to the user has to be selected therefore there are two selection criteria used and they are explained latter in this section: (i) Controller selection criteria (f_{c_i}) and (ii) User's controller selection criterion (f_{k_c}).

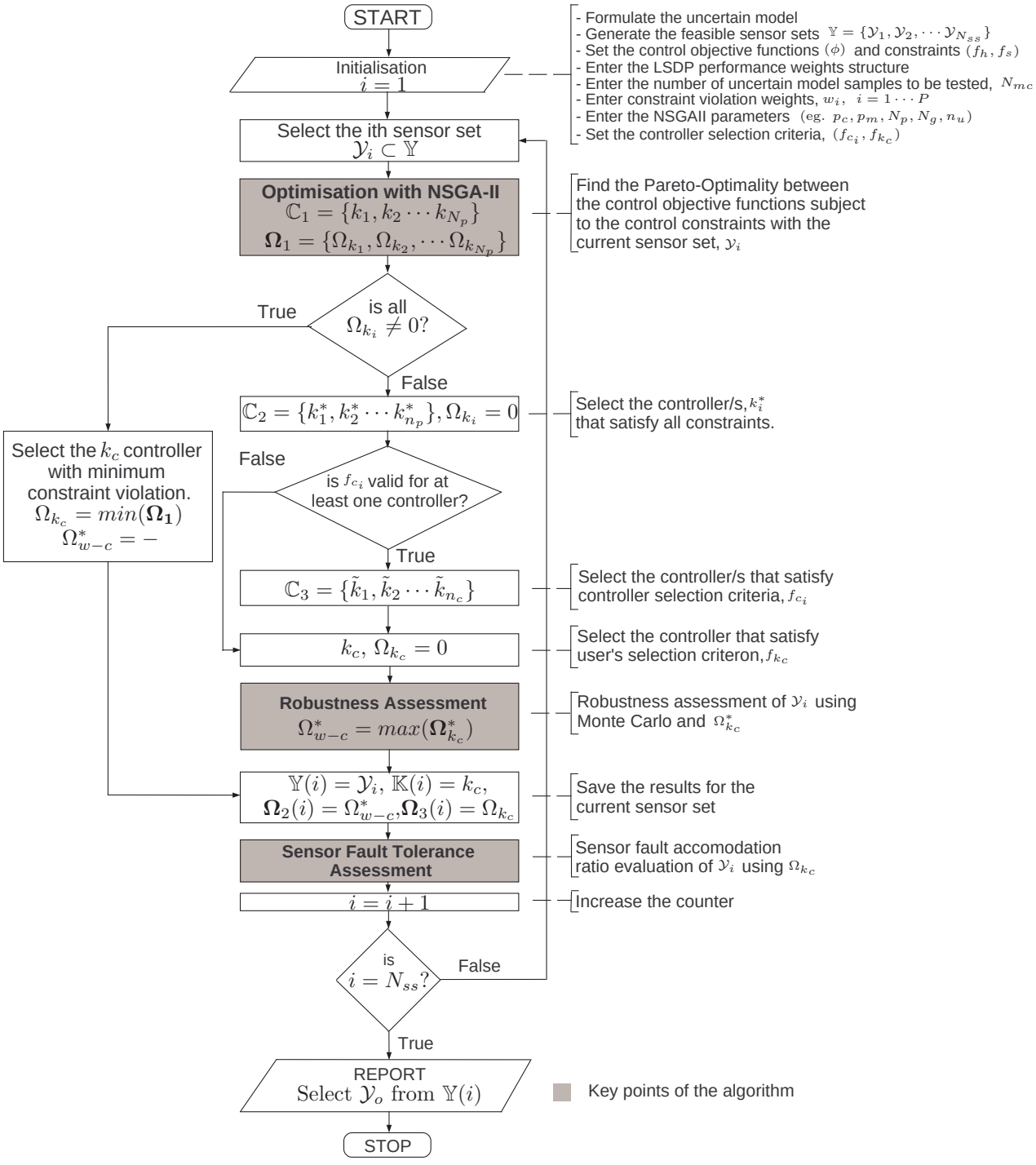

Figure 3: Flowchart of the proposed sensor optimisation framework with robust $\mathcal{H}_\infty$ loop-shaping design.

Starting the optimisation procedure, the first sensor set, ($\mathcal{Y}_1$) is selected and the evolutionary algorithm seeks the Pareto-optimality of the objective functions ϕ_i subject to the control constraints (f_h, f_s). At the end of this stage there is a set of optimally tuned controller $\mathbb{C}_1$ and a set of **O**verall **C**onstraint **V**iolation **F**unctions (OCVFs), $\mathbf{\Omega}_1$ consisting of the Ω_{k_i} (see (18) in Section 4) one for each controller both sets lengths equal to the number of population N_p.

In the sequence, the algorithm seeks to select the 'best' controller. At this point there are two paths to follow:

(i) If there is no controller to satisfy the performance (this can be easily verified by checking the OCVF, Ω_{k_i} in $\mathbf{\Omega}_1$ for each individual response) then the controller, k_c which gives the minimum Ω_{k_i} is selected and saved in $\mathbb{K}(i)$. Ω^*_{w-c} is not evaluated in this case.

(ii) Those controllers satisfying Ω are collected in $\mathbb{C}_2$. The next step is to collect in $\mathbb{C}_3$ the controllers that satisfy the controller selection criteria f_{c_i}. Finally, the user's controller selection criteria, f_{k_c} is used to select the controller, k_c which results in the desired closed-loop response. If no controller exists to satisfy f_{c_i} then the algorithm directly selects a controller based only on f_{k_c}.

The particular sensor set in combination with the selected controller provide a nominal performance that is assessed for parametric uncertainties by combining the MC method using the WOCVF as explained in Section 4 in the following way:

(i) For every q^{th} among the N_{mc} samples of the uncertain EMS system calculate the WOCVF, $\Omega^*_{k_c,q}$.

(ii) From the closed-loop responses of the N_{mc} model samples that result to a set of WOCVF, ie. $\mathbf{\Omega^*_{k_c}}$, the maximum value of $\Omega^*_{k_c}$ is assigned to the current sensor set as the assessment of the worst-case response of the uncertain model. In case the closed-loop response with any sampled model is unstable, $\Omega^*_{k_c}$ is quantified as infinity.

In this way the robustness of the optimally tuned nominal controller, k_c, is assessed.

The next step for the i^{th} sensor set optimisation, is for the proposed algorithm to save the $\mathcal{Y}_i$ in $\mathbb{Y}(i)$, k_c in $\mathbb{K}(i)$, Ω^*_{w-c} in $\mathbf{\Omega}_2(i)$ and Ω_{k_c} in $\mathbf{\Omega}_3(i)$.

Following that, the evaluation of the selection criterion for optimum sensor fault tolerance is done. At this stage the **S**ensor **F**ault **A**ccomodation **R**atio (SFAR) is evaluated which indicates at which percentage the faults can be recovered in sense of the number of fault conditions that could be accommodated by using the remaining healthy sensors in a given sensor set $\mathcal{Y}_i$. Assuming that the sensor set $\mathcal{Y}_i$ has the $\Omega_{k_c} \neq 0$ then the SFAR=0 otherwise SFAR is calculated using the following formula:

$$SFAR(\mathcal{Y}_{i,\Omega_{k_c}=0}) \cong \frac{N_{\mathbb{Y}_{h,\Omega_{k_c}=0}}}{N_{\mathbb{Y}_f}} 100(\%) \tag{1}$$

where $\mathbb{Y}_h$ is the healthy sensor sub-sets of $\mathcal{Y}_i$ that have $\Omega_{k_c} = 0$ and $\mathbb{Y}_f$ are the possible sensor sub-sets that could happen in $\mathcal{Y}_i$ (assuming that is not possible to loose all sensors). $N_{\mathbb{Y}_h}$ and $N_{\mathbb{Y}_f}$ are the number of the sensor sets in $\mathbb{Y}_h$ and $\mathbb{Y}_f$ respectively. Then, $\mathbb{Y}_h$ are the healthy sensor sets in $\mathcal{Y}_i$ that can be successfully used for maintaining the performance under any sensor fault combination that could occur in $\mathcal{Y}_i$. A typical detailed example on the SFAR calculation is found in Appendix A. SFAR metric can be used for optimum sensor set selection that offers the highest degree of fault tolerance against sensor failures.

Next, increase the counter i and moves to the next feasible sensor set until $i = N_{ss}$. At the final end a detailed report is given by the framework that is analysed, in this paper from the simulations of an EMS system.

3. The Single-stage EMS system

3.1. The Non-linear model and linearization

The single-stage, one degree-of-freedom model of the EMS system represents the quarter of a typical MAGLEV vehicle. In order to design a control system with optimum performance using linearized controllers, a careful and rigorous modelling analysis is required and given in this section.

Single-stage electro-magnetic suspension as the one used on the Birmingham Airport MAGLEV and which operated for 12 years in the 1980s and 1990s is suitable for low speed vehicles [30]. The EMS is a non-linear, inherently unstable system with non-trivial control requirements.

The basic quarter car diagram of the MAGLEV vehicle is shown in Fig. 4. The suspension consists of an electromagnet with a ferromagnetic core and a coil of N_c turns which is attracted to the track that is made of ferromagnetic material. The carriage mass (M_c) is supported on the electromagnet, with z_t being the track's position and z the electromagnet's position (both are given as the small variations around the operating point). The distance between them is the airgap, $(z_t - z)$. The airgap is to be kept as closed as possible to the operating point at values that will not exceed the maximum allowed as given later in this section. There are four important variables in an

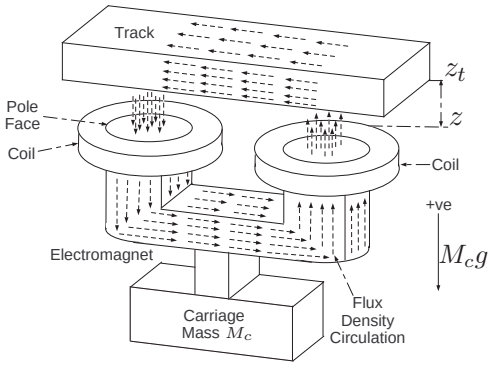

Figure 4: Single-stage suspension for MAGLEV vehicles.

electromagnet named as force F, flux density B, airgap G and the coil's current I that give non-linear characteristics to the suspension as depicted in Fig. 5 [29]. The straight lines show the theoretical relationships and the dashed lines indicate the effects of magnetic saturation in the magnet core. Assuming that the vertical downwards motion is taken as positive the non-linear model of the EMS system is described by: (i) Newton's equation of motion given in (2), (ii) the coil's voltage V_c given in (3) across the electromagnet's coil from Kirchoff's law and (iii) the equations in (4), (5) and (6)

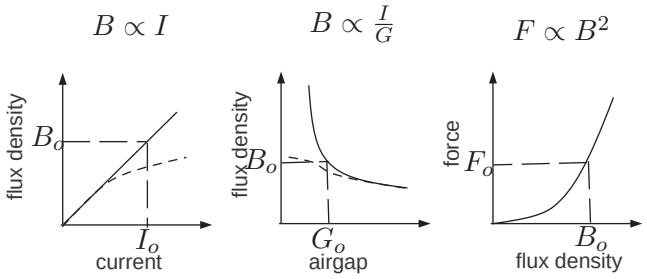

Figure 5: Relationship between the key variables describing the magnet.

that give the force, the flux density and the airgap velocity respectively.

$$M_c \frac{d^2 Z}{dt^2} = M_c g - F \tag{2}$$

$$V_c = I R_c + L_c \frac{dI}{dt} + N_c A_p \frac{dB}{dt} \tag{3}$$

$$B = K_b \frac{I}{G}, \tag{4}$$

$$F = K_f B^2 \tag{5}$$

$$\frac{dG}{dt} = \frac{dz_t}{dt} - \frac{dZ}{dt} \tag{6}$$

where R_c and L_c are the coil's resistance and inductance respectively, A_p is the pole face area and constants K_b, K_f and g are the flux, force and gravity constants with values equal to 0.0015, 0.0221 and $9.81 m/s^2$ respectively.

The linearisation of the EMS is based on small variations around the operating point. The following definitions are used with lower case letters defining the small variations and subscript 'o' referring to the operating point.

$$B = B_o + b, F = F_o + f \tag{7}$$

$$I = I_o + i, G = G_o + (z_t - z) \tag{8}$$

$$V_c = V_o + u_c, Z = Z_o + z \tag{9}$$

Following the linearization procedure described by Michail (2009) [29] the following linearised equations describe the linear model of the EMS:

$$M_c \frac{d^2 z}{dt^2} = -2K_f \frac{I_o}{G_o^2} i + 2K_f \frac{I_o^2}{G_o^3} (z_t - z) \tag{10}$$

$$\frac{di}{dt} = -\frac{R_c i}{L_c + \frac{K_b N_c A_p}{G_o}} + \frac{K_b N_c A_p I_o}{G_o^2 \left(L_c + \frac{K_b N_c A_p}{G_o} \right)} \frac{dz_t}{dt} - \frac{K_b N_c A_p I_o}{G_o^2 (L_c + \frac{K_b N_c A_p}{G_o})} \frac{dz}{dt} + \frac{u_c}{L_c + \frac{K_b N_c A_p}{G_o}} \tag{11}$$

$$\frac{d(z_t - z)}{dt} = \frac{dz_t}{dt} - \frac{dz}{dt} \tag{12}$$

Given the states as $x = [i \quad \dot{z} \quad (z_t - z)]^T$, the state space description of the EMS system can be expressed as in (13). The output equation, y corresponds to i the coil's current, b the flux density, $(z_t - z)$ the airgap, $\dot{z}$ the vertical velocity and $\ddot{z}$ the vertical acceleration.

$$\begin{aligned} \dot{x} &= Ax + B_{u_c} u_c + B_{\dot{z}_t} \dot{z}_t \\ y &= Cx \end{aligned} \tag{13}$$

The matrices A,B_{u_c},$B_{\dot{z}_t}$ and C are given by (14)-(16).

$$A = \begin{bmatrix} -\frac{R_c}{L_c + \frac{K_b N_c A_p}{G_o}} & -\frac{K_b N_c A_p I_o}{G_o^2 \left(L_c + \frac{K_b N_c A_p}{G_o}\right)} & 0 \\ -2K_f \frac{I_o}{M_c G_o^2} & 0 & 2K_f \frac{I_o^2}{M_c G_o^3} \\ 0 & -1 & 0 \end{bmatrix} \tag{14}$$

$$B_{u_c} = \begin{bmatrix} \frac{1}{L_c + \frac{K_b N_c A_p}{G_o}} \\ 0 \\ 0 \end{bmatrix}, B_{\dot{z}_t} = \begin{bmatrix} \frac{K_b N_c A_p I_o}{G_o^2 \left(L_c + \frac{K_b N_c A_p}{G_o}\right)} \\ 0 \\ 1 \end{bmatrix} \tag{15}$$

$$C = \begin{bmatrix} 1 & 0 & 0 \\ \frac{K_b}{G_o} & 0 & -\frac{K_b I_o}{G_o^2} \\ 0 & 0 & 1 \\ 0 & 1 & 0 \\ -2K_f \frac{I_o}{M_c G_o^2} & 0 & 2K_f \frac{I_o^2}{M_c G_o^3} \end{bmatrix} \tag{16}$$

Using the output matrix, C different combination of sensors can be obtained for feedback to the controller defined as the 'sensor set'.

The electromagnet design of MAGLEV vehicles is described in more details by [31]. In this paper, a typical quarter car vehicle of $1000kg$ is studied. It requires an operating force of $F_o = M_c \times g$ and operating airgap (G_o) of $15mm$ in order to accommodate effects from the track roughness. According to these requirements the rest of the electromagnet's parameters listed in Table 1 can be calculated.

Additionally, the EMS system is characterised by uncertainties that can be caused due to various reasons i.e. temperature change, mass change etc. The maximum boundaries of the uncertainties that could possibly occur are listed in Table 1. The subscript 'o' indicates that the variable is at the value of the operating point.

3.1.1. Total Number of Sensor Sets

The total number of sensor sets, N_{ss}, in $\mathbb{Y}$, is calculated from $N_{ss} = 2^{n_s} - 1$. Given that the EMS has 5 sensor outputs, 31 candidate sensor sets, $\mathcal{Y}_i$, can be obtained using combination of the rows of the output matrix, C. However, since the $\mathcal{H}_\infty$ LSDP controller design technique is used in this paper, the airgap measurement is used as a standard measurement and therefore the number of candidate sensor sets ,$\mathcal{Y}_i$, reduces to 16 with the full sensor set given as i.e. $\mathcal{Y}_{16} = \{i, b, (z_t - z), \dot{z}, \ddot{z}\}$.

Table 1: Parameters of the EMS system.

Parameter	Value	Uncertainty
Operating point		
Airgap, G_o	$0.015m$	$\pm 10\%$
Flux density, B_o	$1T$	$\pm 10\%$
Current, I_o	$10A$	$\pm 10\%$
Input voltage, V_o	$100V$	0%
Force, F_o	$9810N$	$\pm 10\%$
Electromagnets' parameters		
Carriage Mass, M_c	$1000kg$	$\pm 10\%$
Coil's Resistance, R_c	10Ω	$\pm 50\%$
Coil's Inductance, L_c	0.1H	$\pm 50\%$
Number of turns, N_c	2000	0%
Pole face area, A_p	$0.01m^2$	0%

3.2. Disturbance inputs to the EMS

3.2.1. Stochastic input

The stochastic inputs are random variations of the track vertical position as the vehicle moves along the track. This is caused by the track installation discrepancies due to track-laying inaccuracies and unevenness. Considering the vertical direction, the velocity variations can be approximated by a double-sided power spectrum density expressed as $S_{\dot{z}_t} = \pi A_r V_v$ [32]. V_v is the vehicle speed (taken as $15m/s$) and A_r represents the track roughness that is given a realistic value for high quality track $1 \times 10^{-7}m$. The corresponding autocorrelation function is given as $R(\tau) = 2\pi^2 A_r V_v \delta(\tau)$ where $\delta(\tau)$ is a dirac delta function.

3.2.2. Deterministic input

Another disturbance input to the EMS system is the position change of the track, z_t, while the vehicle is running caused by the intended changes of the track's inclination. This intended input is due to the track gradients due to the pre-designed infrastructure of the maglev vehicle and is considered the only deterministic input to the suspension in the vertical direction. This transition onto the track's gradient is simulated by the signal depicted in Fig. 6. In this work, a deterministic input with a track gradient of 5% at a vehicle speed of $15m/s$, an acceleration of $0.5m/s^2$ and a jerk of $1m/s^3$ is used.

3.3. Performance requirements of the EMS control system

The control design requirements of an EMS system depend on the type and speed of the train [33, 30]. Typically, the EMS should be able to follow the gradient onto the track (deterministic input) and reject the random variations of the track. Fundamentally, there is a trade-off between the deterministic and stochastic closed-loop responses of the EMS system. The optimisation of the performance is taken as minimisation of the stochastic characteristics subject to control constraints that includes the deterministic and stochastic maximum allowable bounds. The control objectives

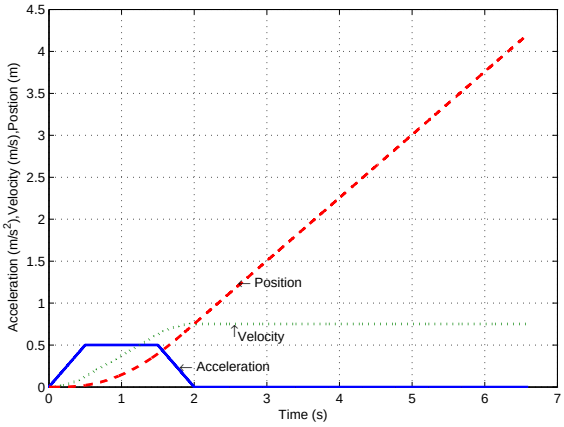

Figure 6: Deterministic input to the suspension with a vehicle speed of $15ms^{-1}$ and 5% track's gradient.

to be minimized are the RMS vertical acceleration $\ddot{z}_{rms}$ and the RMS current variations i_{rms} subject to the control constraints listed in Table 2. This means that the trade-off between $\ddot{z}_{rms}$ and i_{rms} will give the trade-off between the ride quality and input power while the deterministic response will keep the bounds within safe bounds.

The robust stability margin, ϵ (robustness margin) calculated from the LSDP is set to be maximized for maximum robustness against the uncertainties (note that $\gamma = 1/\epsilon$).

Another objective function taken into consideration is the level of the noise $u_{n_{rms}}$ that appears on the input voltage u_c. The level of the noise at the output of a sensor depends on the sensor characteristics itself and the picked-up interference from the surrounding environment. Although the sensors are designed to have noise immunity they still produce noise at the output. Thus an amount of this noise will appear on u_c which effectively affects the $(z_t - z)$. The dynamical behaviour of the EMS has low pass filter characteristics so most of this noise is filtered but it still affects the performance of the suspension if its not kept at low levels [34]. Hence, level of the noise at the input voltage is added as the 4^{th} objective to be minimized i.e $\phi_4 = u_{c_{rms}}$. This help the GA to take it into account during the controller optimised design. $u_{c_{rms}}$ is also included in the controller selection criteria f_{c_i} in order to make sure that is particularly constrained to an up to $10V_{rms}$. In order to measure $u_{c_{rms}}$ an extra simulation is executed with idle track profile i.e. $z_t = 0$ and since there is no exact information about the sensor noise, the noise covariance is typically taken as 1% of the maximum value of the deterministic response of the suspension for the corresponding measured signal.

Summarizing, the objective functions ϕ_i to be minimized are formally written as:

$$\phi_1 = i_{rms},\ \phi_2 = \gamma,\ \phi_3 = \ddot{z}_{rms},\ \phi_4 = u_{n_{rms}} \tag{17}$$

4. Multi-objective constrained optimization

NSGA-II is an evolutionary process that requires some parameters to be assigned in order to ensure proper population convergence towards the Optimum Pareto front between the objective

Table 2: Control constraints on the EMS system.

	EMS limitations	Value
Stochastic Track profile		
f_{s_1}	RMS acceleration, $\ddot{z}_{rms}$	$\leq 1ms^{-2}$
f_{s_2}	RMS airgap variation, $(z_t - z)_{rms}$	$\leq 5mm$
f_{s_3}	RMS control effort, $u_{c_{rms}}$	$\leq 300V(3I_0R_c)$
Deterministic Track profile		
f_{s_4}	Maximum airgap deviation, $(z_t - z)_p$	$\leq 7.5mm$
f_{s_5}	Control effort, u_{c_p}	$\leq 300V(3I_0R_c)$
f_{s_6}	Settling time, t_s	$\leq 3s$
f_{h_1}	Airgap steady state error, $(z_t - z)_{e_{ss}}$	$= 0$
Other constraints		
f_{s_7}	Robust stability margin, ϵ	≥ 0.15

f_{s_i}-Soft constraint, f_{h_i}-Hard constraint

functions. These are mainly selected from experience rather than from a-priori knowledge of the optimisation problem. The crossover probability is generally selected to be large in order to have a good mix of genetic material. The crossover probability, p_c is set to 90% and the mutation probability, p_m is defined as $1/n_u$ where, n_u is the number of variables. The population consists of 50 chromosomes ($N_p = 50$) and the stopping criterion is the maximum generation number N_g. N_g has a significant role on the Pareto-Optimality and the computational time therefore proper selection of N_g is vital. It depends among other factors on the number of variables to be tuned because the larger the n_u the larger the N_g is required with the expense of having longer computational time. The number of variables varies according to the number of sensors hence the N_g varies dynamically. It is set at 250 for sensor sets with up to 2 sensors and for the rest including the full sensor set is set at 300 generations.

In order to achieve the control constraints as described in Section 3.3 a constraint handling technique is necessary. Different constraint handling methods have been developed as described in [35]. The dynamically updated penalty function approach is used in this work. A rigorous description of this method is given in [36]. A function is used in order to 'guide' the objective functions in (17) towards the Pareto-optimality while the control constraints listed in Table 2 are satisfied. The OCVF is given as

$$\Omega_{k_i}(f_s^{(j)}, f_h^{(q)}) = \sum_{j=1}^{J} \omega_j(f_s^{(j)}) + \sum_{q=1}^{Q} \psi_q(f_h^{(q)}) \tag{18}$$

where, ω_j is the j^{th} soft constraint violation for the corresponding j^{th} quantity to be constrained (f_s) and J is the total number of soft constraints. Similarly, ψ_q is the hard constraint violation for the q^{th} quantity to be constrained (f_h) and Q is the total number of hard constraints.

The OCVF not only serves as constraint handling technique but also serves other purposes as described in Section 2.2: (i) as nominal performance indicator, (ii) level of sensor fault tolerance

and (iii) robustness assessment with MC. For the first two properties is straight forward but for the third is described next.

For the robustness assessment (18) is modified as follows

$$\Omega^*_{k_c}(f_s^{(j)}, f_h^{(q)}) = \sum_{j=1}^{J} J w_j \omega_j(f_s^{(j)}) + \sum_{q=1}^{Q} Q \widetilde{w}_q \psi_q(f_h^{(q)}) \tag{19}$$

where w_j and $\widetilde{w}_q$ are the CVWs, for the soft and hard constraints respectively. Depending on the design engineer, the two CVWs can be treated as a set of unified weights or separately. There is no a single systematic method to do that and it depends on the design engineer. However, in this work they are unified and the authors will propose a simple and effective analytical method to calculate them.

The reason for using CVWs is because not all constraints have the same significance i.e. effect on the closed-loop performance. For example if there is a small violation on the airgap deflection $(z_t - z)$ it is not as important as having the same violation on the input voltage, u_c. Therefore weights are assigned to emphasise the difference in the constraint violation. During the MC simulation tests, the WOCVF is evaluated with infinity (∞) if the closed-loop response of the EMS system becomes unstable.

The control constraints are separated into bands of importance as depicted in Fig. 7. The lower band contains the least significance constraints while the top band contains the most significant ones. There are $1, 2, 3 \ldots P$ bands, λ_p are the set of the assigned control constraints in the p^{th} band, n_p is the number of control constraints in the λ_p and w_p and α_p are the weight and the weighting parameter for p^{th} band with the lower having the value of one ($\alpha_1 = 1$).

The weighting, w_i for each band is calculated as follows:

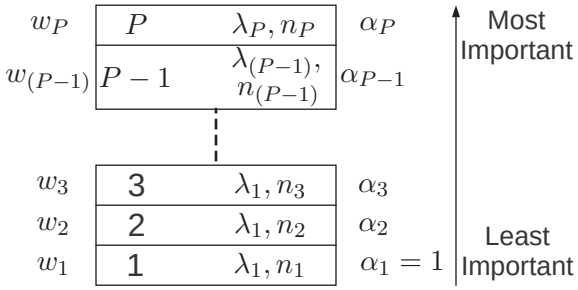

Figure 7: Control constraints weighting assignment.

The weighting values are then given with respect to the weight of the lowest band that have the

smallest weighting parameter:

$$\begin{aligned} w_2 &= \alpha_2 w_1 \\ w_3 &= \alpha_3 w_1 \\ w_4 &= \alpha_4 w_1 \\ &\vdots \\ w_P &= \alpha_P w_1 \end{aligned} \tag{20}$$

(21)

weights and weighting parameters can be written in a series of summation to be equal to one

$$\sum_{p=1}^{P} n_p \alpha_p w_1 = 1 \tag{22}$$

from where the fist CVW, w_1 can be calculated as:

$$w_1 = \frac{1}{\sum_{p=1}^{P} n_p \alpha_p} \tag{23}$$

Then, the i^{th} CVW w_i can be calculated as

$$w_i = \frac{\alpha_i}{\sum_{p=1}^{P} n_p \alpha_p}, i = 1 \cdots P \tag{24}$$

For the EMS system the control constraints are divided into three bands, i.e. $P = 3$. The control constraints listed in Table 2 are assigned to each band as follows $\lambda_1 = \{t_s, (z_t - z)_{e_{ss}}\}$, $\lambda_2 = \{u_{c_p}, u_{c_{rms}}, \epsilon, \ddot{z}_{rms},\}$ and $\lambda_3 = \{(z_t - z)_p, (z_t - z)_{rms}\}$ therefore $n_1 = 2$, $n_2 = 4$ and $n_3 = 2$. The weighing parameters can be assigned taking into account that λ_1 is of low importance λ_2 is of medium importance and λ_3 is of the highest importance. Hence, since $\alpha_1 = 1$ the α_2 and α_3 weighting parameters are selected to be $\alpha_2 = 5, \alpha_3 = 25$. This means that the set of constraints in λ_2 are 5 times and λ_3 are 25 times 'more important' that the ones in λ_1. These values are generated ad-hoc but a formula can be used if many bands exits i.e. the weighting parameter for the i^{th} band can be calculated as $\alpha_i = \beta^{i-1}$ where β is a free selected integer greater than one. From the data above the CVW are calculated as $w_1 = 0.0139, w_2 = 0.0694$ and $w_3 = 0.347$.

5. Sensor fault tolerance via LSDP design and robustness assessment

Sensor failures occur often in engineering systems reducing the reliability of a control system and thread the integrity of safety-critical systems. In this paper, the AFTC concept is used to accommodate sensor failures in combination with the proposed framework.

The AFTC scheme composes of a bank of $\mathcal{H}_\infty$ LSDP designed controllers, the **F**ault **D**etection and **I**solation unit and Reconfiguration mechanism. The overall mechanism is applied on the non-linear model of the EMS system with the operating point defined in Table 1 [37]. The diagram which describes the sensor fault tolerant control concept is depicted in Fig. 8.

When multiple sensor faults occur the faulty sensors are detected and isolated. After that, controller reconfiguration follows in order to switch to another controller that is tuned for the remaining healthy sensors (sub-set of the selected sensor set). Note that for simplicity the switching delay is assumed to be negligible. In order to detect multiple faults, the FD mechanism monitors the

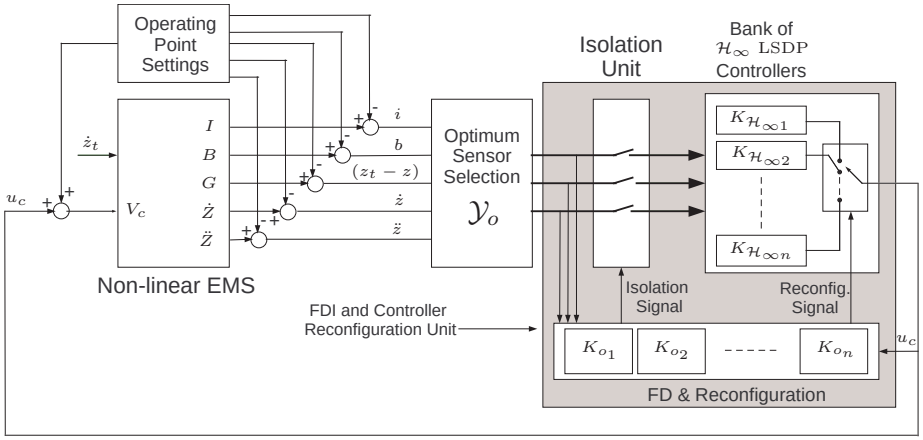

Figure 8: AFTC diagram for multiple sensor failures using a bank of $\mathcal{H}_\infty$ LSDP controllers.

residual from each healthy sensor. The residual for each healthy sensor is typically produced by means of dedicated observers [38]. Therefore, for each sensor set there are one controller and one observer. Hence a bank of dedicated observers (i.e. $K_{o_1}, K_{o_2}....K_{o_n}$) is used for fault detection. Each time that faults happen, the reconfiguration mechanism gives a signal to reconfigure the controller, the dedicated observers as well as isolate the faulty sensors. Isolating the faulty sensors is done by taking the sensor out of the loop in such a way that the faulty signal is not fed into the new controller (i.e. can be done using switches).

The nominal design of the $\mathcal{H}_\infty$ controller is based on the normalised coprime-factor plant description as proposed by [8], which incorporates the simple performance/robustness tradeoff obtained in loop-shaping, with the normalised Left Coprime Factorisation (LCF) robust stabilization method as a means of guaranteeing the closed-loop stability.

Controller design using the so called loop-shaping design procedure (LSDP) requires the linearized model of the plant to be controlled (for the EMS system, the linear time-invariant state space model in (13) is used in the design) and is done in two steps. The first is shaping the open-loop characteristics of the plant using pre and post weighting functions, W_1 and W_2 as shown in Fig. 9(a). The plant is temporarily redefined as $\hat{G}(s) = W_2 G W_1$ and the $\mathcal{H}_\infty$ optimal controller $\hat{K}(s)$ is calculated. In the second step the weighting functions are merged with the controller by defining the overall controller $K(s) = W_1 \hat{K} W_2$ as shown in Fig. 9(b). The size of model uncertainty is quantified by the stability radius ϵ i.e. the stability margin [8, 7]. For values of $\epsilon \geq 0.25$, 25% coprime factor uncertainty is allowable. However, in this paper a relaxed stability margin is used set at $\epsilon \geq 0.15$.

The vital part of the LSDP is the performance weights whose structures and bounds to be varied are selected by the user of the framework. In order to achieve the desired optimum performance those weights are optimally tuned using the NSGAII. This is an iterative process where the bounds

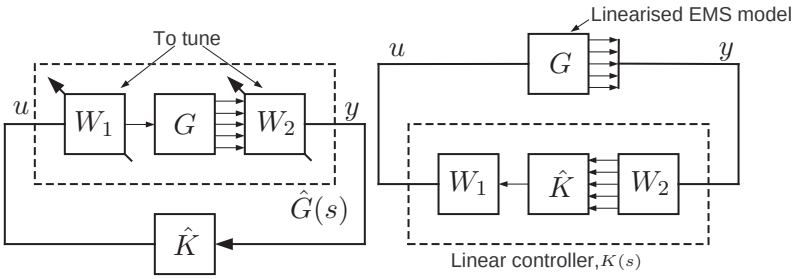

(a) *Shaped plant.* **(b) *Final controller.***

Figure 9: $\mathcal{H}_\infty$ loop-shaping controller design.

of the weights are randomly varied until the optimum performance is achieved.

In typical design the structure of the performance weights and thus the controller are to be kept as simple as possible. Thus, the W_1 pre-compensator, is chosen as a single scalar performance weight set to unity. For the W_2 post-compensators there can be five weighting functions that are used depending on the selected sensor set. The airgap $(z_t - z)$ measurement is a compulsory measurement required for proper control of the magnet distance from the rail and thus a low pass filter $(W_{(z_t-z)})$ is chosen with integral action allowing zero steady state airgap error. The performance weights used in this paper are given as

$$W_1 = 1; \quad W_2 = diag(W_i, W_b, W_{(z_t-z)}, W_{\dot{z}}, W_{\ddot{z}}) \tag{25}$$

with,

$$W_{(z_t-z)} = \left(\frac{\frac{s}{M_w^{1/n_w}} + \omega_w}{s + \omega_w A_w^{1/n_w}} \right)^{n_w} \tag{26}$$

The low pass filter results to a minimum phase and stable performance weight $W_{(z_t-z)}$, with roll-off rate n_w. M_w is the high frequency gain, A_w the low frequency gain and ω_w the crossover frequency. Details for weighting function selection for the loop-shaping design can be found in [18, 7].

Taking advantage of the fact that any changes in the closed-loop response (both stability and performance) will be reflected on the WOCVF, $\Omega^*_{k_c}$ in (19), robustness against parametric uncertainties can be tested when is combined with MC technique.

Monte Carlo is a probabilistic method that is used to randomly sample an uncertain variable with a given probability distribution. There are many distribution functions that can be used to sample an uncertain variable. The structured uncertainties of the EMS system are listed in Table 1 and they are assumed to be uniformly sampled. The probability density function used for each uncertain parameters is illustrated in Fig. 10 and expressed in (27). Θ_o, Θ_{min} and Θ_{max} are the mean, the minimum and the maximum values of the uncertain parameter respectively and $U(\Theta)$ is the probability of each variable.

$$U(\Theta) = \begin{cases} U_m = 1/(\Theta_{max} - \Theta_{min}) & if \ \Theta_{min} \leq \Theta \leq \Theta_{max} \\ 0 & if \ \Theta_{min} > \Theta > \Theta_{max} \end{cases} \tag{27}$$

As illustrated in Fig. 11 the nominal controller is tested under N_{mc} multiple samples of the EMS model producing a vector of WOCVFs, $\mathbf{\Omega}_i, i = 1 \cdots N_{mc}$ from where the worst-case WOCVF is selected, i.e. $\Omega^*_{w-c} = max(\mathbf{\Omega}^*_{k_c})$. The Ω^*_{w-c} is the worst case performance that can happen among the N_{mc} model samples.

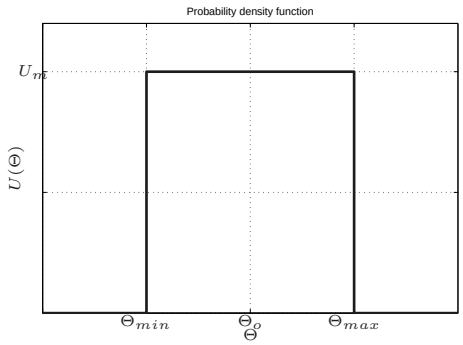

Figure 10: Uniform probability distribution function.

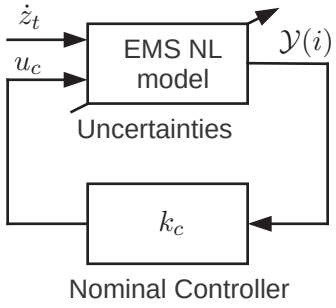

Figure 11: Monte Carlo test of the nominal optimally tuned LSDP designed controller.

6. Framework assessment and data analysis

The framework is tested in MATLAB R2009b simulation environment without Java function due to large computational need (simulation based). The computer used is the powerful DELL T610 with 2.93GHz Intel®Xeon®X5570 processor and 8GB RAM. The average simulation time per sensor set is about 5.5 hours while completion of the framework takes around 87 hours.

The controller selection criteria (f_{c_i}, f_{k_c}) for the desired closed-loop response are given as follows

$$f_{c1} \equiv \ddot{z}_{rms} \leq 0.5m/s^2, f_{c2} \equiv u_{n_{rms}} \leq 10V, \tag{28}$$

$$f_{k_c} \equiv max(\epsilon) \tag{29}$$

The first set of closed-loop desired characteristics in (28) ensures that the controllers to be selected are within the limits indicated. f_{k_c} in (29) ensures that the selected controller has the maximum robust stability margin (maximum robustness).

Table 3 lists the detailed results from the framework execution. The second column lists the

sensor sets and the first the corresponding identification number. The next four columns are the variables from the closed-loop response with the stochastic track profile and the further four lists the variable values from the deterministic track profile. The next is the rms value of the noise on the driving signal from idle track profile and the following column is the resulting stability margin from the $\mathcal{H}_\infty$ loop-shaping design. The 13^{th} and 14^{th} columns show whether the controller selection criteria in (28) and (29) are satisfied or not. The 15^{th} column shows the SFAR value of each sensor set and 16^{th} column shows whether the OCVF, $\Omega_{k_c} = 0$ (marked as '✓') or not $\Omega_{k_c} \neq 0$ (marked as 'x'). As explained if $\Omega_{k_c} = 0$ then all control constraints are within the pre-set limits otherwise there is one or more control constraint violations marked with bolded fonts. The last column lists the WOCVF, $\Omega^*_{k_c}$. Recall that the WOCVF is evaluated by infinity during the MC test if there is instability in the closed-loop response. The table gives a full picture of the EMS optimum response under multiple circumstances that are rigorously described next.

The proposed systematic framework is able to identify stabilizing controllers that satisfy the OCVF for 15 out of 16 sensor sets. Inspecting columns f_c and f_{k_c} there are 6 sensor sets found that satisfy (28) and (29) i.e. $id : 3$,$id : 8$ and $id : 13 - 16$. Comparing the corresponding sensor set rows with the control constraints listed in Table 2 it can be seen that the optimum nominal performance has been fully satisfied. The f_{c_1} is not satisfied with many sensor sets (i.e. the $\ddot{z}_{rms}$ exceeds the given criterion) but those could be still used for fault tolerance under multiple sensor faults.

Table 3: Optimised sensor configurations for control and sensor fault tolerance of the EMS system.

		Stochastic Input				Deterministic Input				Idle input						
id	Sensor set $\mathcal{Y}_i$	g_{rms}	$u_{c_{rms}}$	$\ddot{z}_{rms}$	i_{rms}	g_p	u_{c_p}	t_s	e_{ss}	$u_{n_{rms}}$	ϵ	f_c	f_{k_c}	SFAR	Ω_{k_c}	$\Omega^*_{k_c}$
		mm	V	ms^{-2}	A	mm	V	s		V						
1	$(z_t - z)$	1.41	37.19	0.77	1.30	1.24	11.92	2.29	✓	0.20	0.15	x	✓	0	✓	∞
2	$i, (z_t - z)$	1.41	37.19	0.77	1.30	1.24	11.92	2.29	✓	0.20	0.15	x	✓	100	✓	∞
3	$b, (z_t - z)$	1.24	24.88	0.47	1.02	3.67	27.50	2.10	✓	0.37	0.26	✓	✓	100	✓	28.45
4	$(z_t - z), \dot{z}$	1.41	37.19	0.77	1.30	1.24	11.93	2.29	✓	0.20	0.15	x	✓	100	✓	∞
5	$(z_t - z), \ddot{z}$	1.41	37.19	0.77	1.30	1.24	11.92	2.29	✓	0.20	0.15	x	✓	100	✓	∞
6	$i, b, (z_t - z)$	1.40	37.35	0.77	1.30	1.23	11.87	2.29	✓	0.20	0.15	x	✓	100	✓	∞
7	$i, (z_t - z), \dot{z}$	1.40	43.19	0.88	1.35	1.06	10.74	2.27	✓	0.12	0.15	x	✓	100	✓	∞
8	$i, (z_t - z), \ddot{z}$	1.01	40.60	0.48	0.87	3.36	25.53	2.15	✓	2.04	0.27	✓	✓	100	✓	1.01
9	$b, (z_t - z), \dot{z}$	1.41	37.19	0.77	1.30	1.24	11.92	2.29	✓	0.20	0.15	x	✓	100	✓	∞
10	$b, (z_t - z), \ddot{z}$	1.41	37.19	0.77	1.30	1.24	11.92	2.29	✓	0.20	0.15	x	✓	100	✓	∞
11	$(z_t - z), \dot{z}, \ddot{z}$	1.28	35.28	0.75	1.18	2.87	22.17	2.08	x	15.98	**0.12**	-	-	-	x	-
12	$i, b, (z_t - z), \dot{z}$	1.41	37.18	0.77	1.30	1.24	11.92	2.29	✓	0.20	0.15	x	✓	100	✓	∞
13	$i, b, (z_t - z), \ddot{z}$	1.16	25.90	0.45	0.96	3.78	28.40	2.13	✓	0.90	0.21	✓	✓	100	✓	0.76
14	$i, (z_t - z), \dot{z}, \ddot{z}$	1.16	25.21	0.42	0.95	4.13	30.78	2.15	✓	0.98	0.24	✓	✓	85.71	✓	0.26
15	$b, (z_t - z), \dot{z}, \ddot{z}$	1.43	20.76	0.45	1.15	4.34	31.86	2.18	✓	0.26	0.18	✓	✓	85.71	✓	12.37
16	$i, b, (z_t - z), \dot{z}, \ddot{z}$	1.00	42.27	0.49	0.86	3.28	25.00	2.15	✓	2.13	0.27	✓	✓	93.33	✓	1.25

$g_p \equiv (z_t - z)_p$, $g_{rms} \equiv (z_t - z)_{rms}$, $e_{ss} \equiv (z_t - z)_{e_{ss}}$

If the user is to consider optimum sensor selection for optimum control of the EMS then the $id:3$ which satisfies f_c, f_{k_c} and Ω_{k_c} with the minimum number of sensors can be used. The parallel coordinate plot represents the Pareto-Optimality of the objective functions with the $id:3$ sensor set $\{b,(z_t-z)\}$ that is found using the NSGA-II. This represents the response of a pool of optimally tuned controllers, $\mathbb{C}_1$, that minimize the functions in (17) subject to the control constants tabulated on Table 2. At the last N_g^{th} generation, of the optimisation the population of the optimised solutions is depicted in Fig. 12(a). The trade-off of the objective functions is illustrated through a parallel coordinate plot. All solutions of each ϕ_i are placed on the vertical axis and connected with N_p straight lines (equal to the number of population) creating the parallel coordinate system which illustrates the trade-off of the minimized objectives. Note that all control constraints are satisfied i.e. all elements $\Omega_{k_i} \in \mathbf{\Omega_1}$ are zero. The objective functions are normalised around one for easy graphical illustration using their maximum values shown on top of the graph.

From this last generation the controller, k_c is selected according to (28) and (29). The response of k_c with the nominal EMS model to deterministic input disturbance (described in Section 3.2) is depicted in Fig. 12(b). The maximum airgap deflection is less than 7.5mm and it settles back to the operating point(15mm) within less than $3s$ with the steady state error being almost zero. The x-axis (zero line) of the figure represents the operating airgap of the suspension. The same graphical representation is used with the rest of suspension's variables in this paper.

Looking at the results from the robust control point of view, optimum sensor selection includes

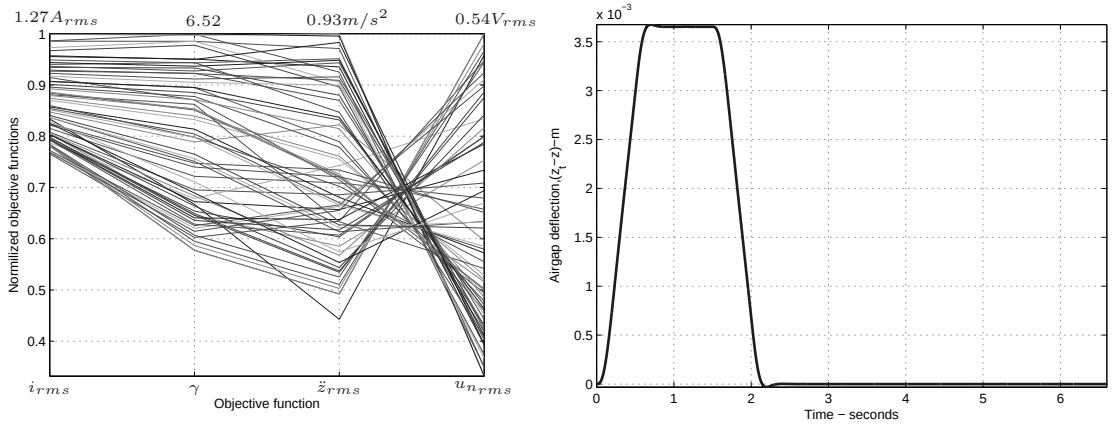

(a) ***Trade-off between the objective functions.*** **(b)** ***Airgap response.***

Figure 12: Parallel coordinates plot showing the trade-off between the objective functions in (17) and airgap response to deterministic input both with $id:3$.

the WOCVF $\Omega^*_{k_c}$ tabulated on Table 4). This means that the $id:3$ with $\Omega^*_{k_c-id:3}=28.45$ cannot be used to accommodate the parametric uncertainties of the EMS since there are very important control constraint violations from both the stochastic and deterministic track profiles.

More useful information from the results are extracted using the WOCVF in the last column. Note that for the sensor sets that do not satisfy the OCVF, the WOCVF is not evaluated. Typically, the lower the value of the $\Omega^*_{k_c}$ is the higher the robustness against the uncertainties is. Looking at the value of $\Omega^*_{k_c}$ for each sensor set it can be seen that it varies from values between 0.26-28. The

detailed results of the candidate sensor sets ($id:3, id:8, id:13-16$) from the corresponding worse case closed-loop performances are listed on the same table. The Table shows the measurements from both the corresponding responses with stochastic and deterministic inputs to the EMS system. The measurements with bolded numbers show that its maximum value is exceeded. $id:3$ has 2 constraint violations (i.e. $(z_t-z)_{rms}, (z_t-z)_p$) with the highest importance (i.e. w_3). Following that option, the $id:15$ with 2 constraint violations, the $(z_t-z)_p$ and t_s where the first is of highest importance (w_3) while the second is of lowest importance (w_1). This explains why both $id:3$ and $id:15$ have the highest $\Omega^*_{k_c}$. The rest of the constraint violations are from the peak values of the input voltage (u_{c_p}) with medium importance (w_2) and from the $(z_t-z)_{e_{ss}}$ with lowest importance (w_1). This results with the lowest $\Omega^*_{k_c}$ for sensor sets with $id:8$, $id:13$, $id:14$ and $id:16$. The

Table 4: Robustness assessment results with Monte Carlo for the EMS system.

		Stochastic Input			Deterministic Input					
		g_{rms}	$u_{c_{rms}}$	$\ddot{z}_{rms}$	g_p	u_{c_p}	t_s	e_{ss}	ϵ	$\Omega^*_{k_c}$
	$w_i \longrightarrow$	w_3	w_2	w_2	w_3	w_2	w_1	w_1	w_2	
id	Sensor set	mm	V	ms^{-2}	mm	V	s	mm		
3	$b, (z_t-z)$	**12.0**	141	0.42	**20.0**	232	2.1	**172**	0.26	28.45
8	$i, (z_t-z), \ddot{z}$	1.5	35.10	0.44	5.0	**847**	2.14	5e-5	0.27	1.01
13	$i, b, (z_t-z), \ddot{z}$	1.3	23.28	0.36	5.5	**344**	2.14	**6.19**	0.21	0.76
14	$i, (z_t-z), \dot{z}, \ddot{z}$	1.7	24.39	0.37	6.3	**440**	2.15	0.0041	0.24	0.26
15	$b, (z_t-z), \dot{z}, \ddot{z}$	4.6	57.21	0.37	**19.0**	219	**3.17**	**69.68**	0.18	12.37
16	$i, b, (z_t-z), \dot{z}, \ddot{z}$	1.4	40.31	0.45	4.8	**976**	2.14	**0.090**	0.27	1.25

$$w_i = \{w_1 = 0.0139, w_2 = 0.0694, w_3 = 0.347\}$$
$$g_p \equiv (z_t-z)_p,\ g_{rms} \equiv (z_t-z)_{rms},\ e_{ss} \equiv (z_t-z)_{e_{ss}}$$

figures in Fig. 13(a) and Fig. 13(b) show the deterministic closed-loop responses of the EMS with the $id:8$ and $id:14$. The responses from both sensor sets fully agrees with the control constraints as given except with the steady state error which is around $1mm$ but this does not threaten the integrity of the system. Looking at the results in Table 3 from the sensor fault tolerance point of view the SFAR and the OCVF are used as a metric select the sensor set which results the optimum performance and have a desired level of fault tolerance. The SFAR is evaluated for most of the sensor sets except the $id:1$ because there is only one sensor and the $id:11$ because the OCVF is not satisfied. Most sensor sets ($id:2-10, id:12-13$) have a SFAR of 100%. The last three sensor sets with larger number of sensors have lower level of sensor fault recovery ratio. Nevertheless, they still offer fault tolerance to up to 93%.

The final step is to select the best sensor set starting with elimination of the sensor sets that do not satisfy Ω_{k_c}, f_c, f_{k_c} and the sensor sets with $\Omega^*_{k_c} = \infty$. After that there are 6 candidate sensor sets: ($id:3, id:8, id:13-16$). From these candidates, its easy to identify that the $id:3$ and $id:15$ have $\Omega^*_{k_c-id:3} = 28.45$ and $\Omega^*_{k_c-id:15} = 12.37$ respectively both excluded although they have SFAR=100%. Finally, from the four left candidates it is easy to identify that the $id:8$ has both the higher SFAR and sufficient robustness with the minimum number of sensors. If better robustness is required the other option is the $id:14$ with $\Omega^*_{k_c} = 0.26$ but with smaller SFAR.

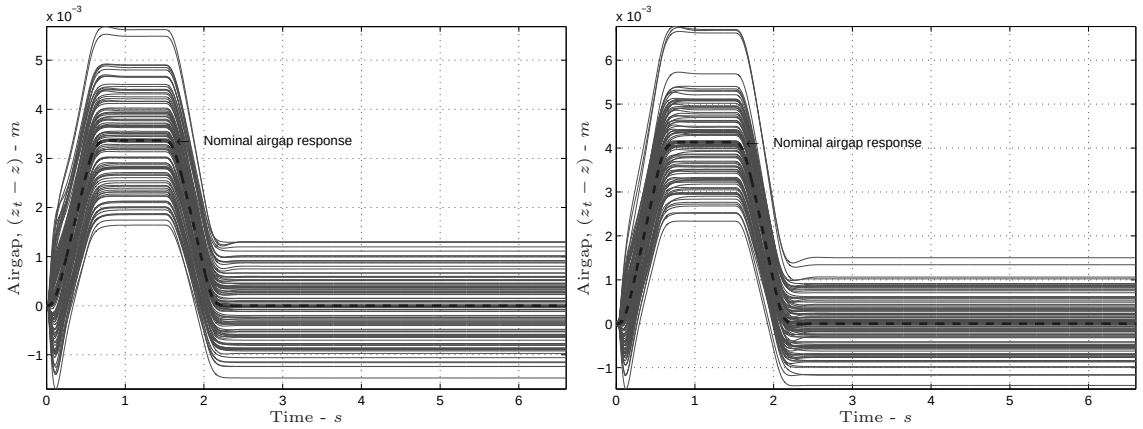

(a) *Airgap deflections with id:8*=$\{i, (z_t - z), \ddot{z}\}$. (b) *Airgap deflections with id:14*=$\{i, (z_t - z), \dot{z}, \ddot{z}\}$.

Figure 13: Airgap deflections (with deterministic track profile) for 100 samples of the non-linear uncertain model.

At this stage, the optimum sensor set selection comes to the point where the selection is relative to the system's requirement and at what level of fault tolerance and robustness is required by the engineer. For the work in this paper, the $id : 8$ is selected to be the optimum set of sensors that can offer 100% sensor fault recovery and robustness with the minimum number of sensors i.e. $\mathcal{Y}_o = \{i, (z_t - z), \ddot{z}\}$. Additionally, the optimum nominal performance is achieved even under multiple sensor faults. At this point it is mentioned that robustness under sensor faults is not quarantined in this version of the framework but is left as future work.

Sensor fault tolerance is a vital issue in control system design because the stability of the system depends on it. The sensor fault modelling can be done in three ways [38]: (i) abrupt fault (stepwise) (i) incipient fault (drift-like) and (iii) intermittent fault. For the simulation tests the first case is assumed in this paper. Since the $\mathcal{Y}_o = \{i, (z_t - z), \ddot{z}\}$ and the airgap measurement is a standard measurement it is assumed that faults can affect the current and the acceleration sensors. Figure 14 illustrates the abrupt-like fault on the accelerometer during the deterministic and stochastic track profiles at $1s$. The output signal is normal until the first second but afterwards the fault is injected having low frequency random characteristics. Similar profile appears on the current sensor after the fault is injected. The sensor fault tolerance based on the diagram in Fig. 8 involves all possible sensor fault conditions that could possibly happen with the i and $\ddot{z}$ and the EMS performance after the controller reconfiguration. The results are listed in Table 5. The first row is the optimum sensor set $id : 8$ and the rest are the healthy sensor sets after faults with the corresponding controllers and EMS performance. The results show that the nominal performance of the EMS system is maintained in both stochastic and deterministic track profiles.

Figure 15 shows the closed-loop response of the EMS system under the worst case scenario where both i and $\ddot{z}$ fail at $1s$. The stability of the system is successfully maintained in both cases. Additionally, the figures show the error of the airgap with fault-free condition and with faults on the aforementioned sensors. The peak-error with the deterministic input is at $2.5mm$ and then it goes to zero while the stochastic response has a small continues error without any significance effect

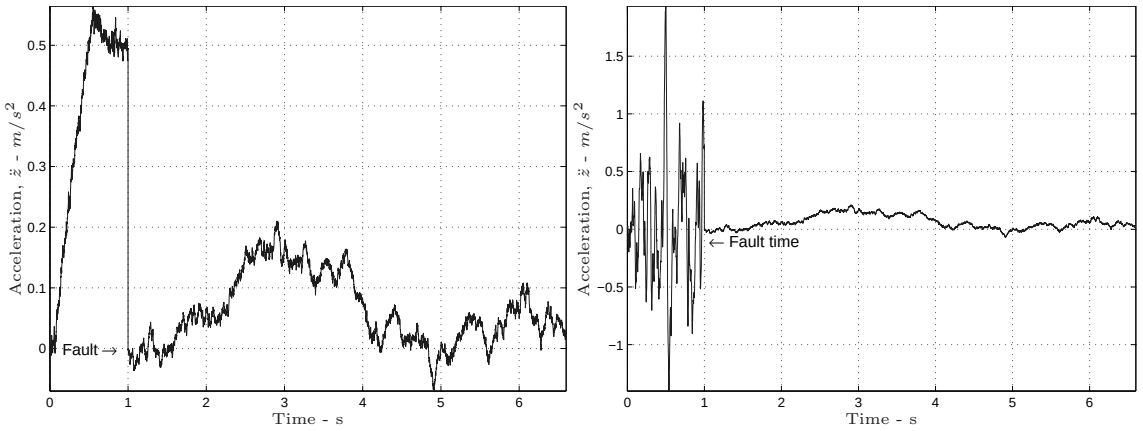

(a) *Fault profile of the acceleration sensor for the deterministic response*

(b) *Fault profile of the acceleration sensor for the stochastic response*

Figure 14: Abrupt fault profiles of the accelerometer sensor in $\mathcal{Y}_o$

Table 5: Possible sensor fault conditions with $\mathcal{Y}_o = id : 8$ and nominal performance recovery.

Healthy Sensor sets, $\mathcal{Y}_{o_h}$	Faulty Sensor Sets, $\mathcal{Y}_{o_f}$	LSDP controller	EMS Performance	
			Deterministic Input	Stochastic Input
$i, (z_t - z), \ddot{z}$	-	$K_{\mathcal{H}_{\infty_1}}^{i,(z_t-z),\ddot{z}}$	✓	✓
$i, (z_t - z)$	$\ddot{z}$	$K_{\mathcal{H}_{\infty_2}}^{i,(z_t-z)}$	✓	✓
$(z_t - z), \ddot{z}$	i	$K_{\mathcal{H}_{\infty_3}}^{(z_t-z),\ddot{z}}$	✓	✓
$(z_t - z)$	$i, \ddot{z}$	$K_{\mathcal{H}_{\infty_4}}^{(z_t-z)}$	✓	✓

on the performance of the EMS.

7. Conclusions

The paper presented an approach for selecting sensor sets for control and fault tolerance on EMS systems, aiming to offer a level of simplicity and flexibility in such a demanding design problem. The computational expensive, off-line framework successfully identifies fallback options in case of multiple sensor faults with minimum sensor redundancy. Advanced software programming, i.e. parallel programming, can alleviate some of the time consuming nature of the framework (which arises due to the complex nature of the problem and related constraints and parameter dependence) by reducing computational effort. It is worth noting that user experience can also relax the issue of parameter dependence. With no loss of generality the framework can be applied to a wider range of engineering systems with multiple conflicting and complex control requirements.

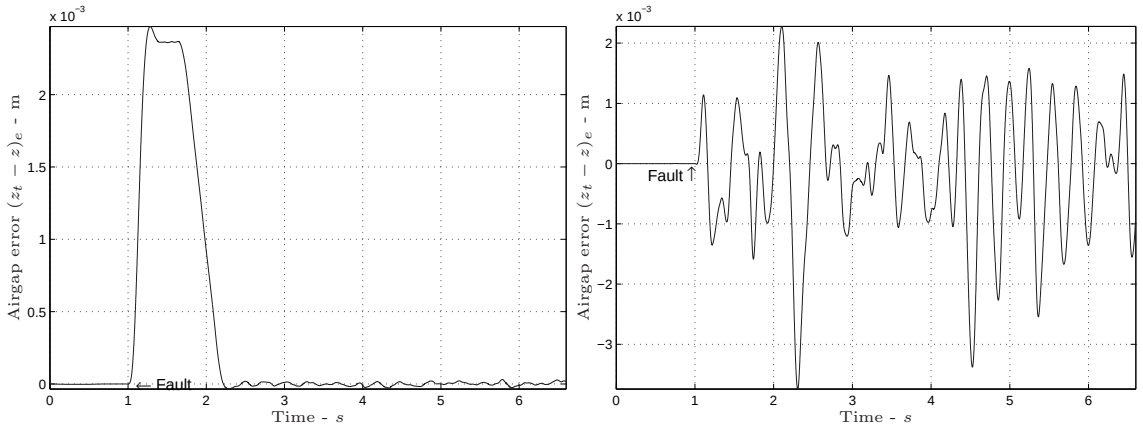

(a) *Response with deterministic input.* **(b) *Response with stochastic input.***

Figure 15: Airgap error $(z_t - z)_e$ between the airgap with fault-free condition $(z_t - z)$ and the airgap under the sensor faults condition $(z_t - z)_f$. Both i and $\ddot{z}$ in the $\mathcal{Y}_o$ $(id : 8)$ simultaneously fail at $1s$.

Acknowledgements

Parts of this research were supported by Engineering and Physical Sciences Research Council in United Kingdom, BAE Systems (Systems Engineering Innovation Center) under project grand ref. EP/D063965/1 and by NEW-ACE EPSRC network under project grand ref. EP/E055877/1. The authors would also like to thank the anonymous reviewers for their rigorous review of this paper that significantly improved the quality of it.

Appendix A. SFAR calculation example

Assume that there are three sensors at the output of a plant to be used for control, i.e. y_1, y_2, y_3. The total number of sensor sets in $\mathbb{Y}_i$ is given by $N_{ss} = 2^{n_s} - 1 = 7$ hence $\mathbb{Y}_i = \{\mathcal{Y}_1, \mathcal{Y}_2, \mathcal{Y}_3, \mathcal{Y}_4, \mathcal{Y}_5, \mathcal{Y}_6, \mathcal{Y}_7\}$. Assume that optimising the performance for each sensor set in $\mathbb{Y}_i$ the SFAR has to calculated for the full sensor set, $\mathcal{Y}_7 = \{y_1, y_2, y_3\}$ must have $\Omega_{k_c} = 0$ (otherwise SFAR is set at zero). Until this stage, Ω_{k_c} in $\mathbf{\Omega}_3$ for each sensor sub-set, (ie. $\mathcal{Y}_{(1-6)}$) is calculated as shown on Table A.7. Note that Ω_{k_c} for $\mathcal{Y}_3$ and $\mathcal{Y}_6$ is not equal to zero indicated by 'x' mark. This means that there are one or more control constraint violation using the corresponding sensor set. If $\Omega_{k_c} = 0$ means that all control constraints are within the pre-set limits and is indicated by '✓'. By definition the SFAR $(\mathcal{Y}_{i,\Omega_{k_c}=0})$ is given by

$$SFAR(\mathcal{Y}_{7,\Omega_{k_c}=0}) \cong \frac{N_{\mathbb{Y}_h,\Omega_{k_c}=0}}{N_{\mathbb{Y}_f}} 100(\%) \tag{A.1}$$

assuming that not all sensors can fail in $\mathcal{Y}_7$, $N_{\mathbb{Y}_f} = 2^{n_{\mathcal{Y}_7}} - 2 = 6$, $n_{\mathcal{Y}_7}$ is the number of sensors in $\mathcal{Y}_7$. Then, $N_{\mathbb{Y}_h,\Omega_{k_c}=0}$ is calculated using a simple iterative algorithm given in Table A.6. In this case is found that SFAR of $\mathcal{Y}_7$ is found to be $SFAR(\mathcal{Y}_{7,\Omega_{k_c}=0}) = (4/6) * 100 = 66.66\%$ which means that 4 sub-sets of $\mathcal{Y}_7$ can be used to restore the performance of the plant with various sensor faults.

Table A.6: SFAR calculation algorithm.

if Ω_{k_c} of $\mathcal{Y}_7$ equal to zero
Set $N_{\mathbb{Y}_{h,\Omega_{k_c}=0}} = 0$, $N_{\mathbb{Y}_f} = 2^{n_{\mathcal{Y}_7}} - 2$
  for i=1 to $N_{\mathbb{Y}_f}$
    if Ω_{k_c} of $\mathcal{Y}_i$ equal to zero
      $N_{\mathbb{Y}_{h,\Omega_{k_c}=0}} = N_{\mathbb{Y}_{h,\Omega_{k_c}=0}} + 1$
    end
  end
$SFAR(\mathcal{Y}_{7,\Omega_{k_c}=0}) = (N_{\mathbb{Y}_{h,\Omega_{k_c}=0}}/N_{\mathbb{Y}_f})100 * \%$
else $SFAR(\mathcal{Y}_{7,\Omega_{k_c}=0}) = 0$
end

Table A.7: Sensor subsets of $\mathcal{Y}_7$ with the corresponding Ω_{k_c}.

$\mathcal{Y}_i$	Sensor sub-sets, of $\mathcal{Y}_7$	Ω_{k_c}
$\mathcal{Y}_1$	y_1	✓
$\mathcal{Y}_2$	y_2	✓
$\mathcal{Y}_3$	y_3	x
$\mathcal{Y}_4$	y_1,y_2	✓
$\mathcal{Y}_5$	y_2,y_3	✓
$\mathcal{Y}_6$	y_1,y_3	x

[1] D. Theilliol, H. Noura, and J-C. Ponsart. Fault diagnosis and accommodation of a three-tank system based on analytical redundancy. *ISA Transactions*, 41(3):365 – 382, 2002.

[2] R.F. Escobar, C.M. Astorga-Zaragoza, A.C. Tllez-Anguiano, D. Jurez-Romero, J.A. Hernndez, and G.V. Guerrero-Ramrez. Sensor fault detection and isolation via high-gain observers: Application to a double-pipe heat exchanger. *ISA Transactions*, 50(3):480 – 486, 2011.

[3] A. Mihankhah, F.R. Salmasi, and K. Salahshoor. Partial and total actuator faults accommodation for input-affine nonlinear process plants. *ISA Transactions*, 52(3):351 – 357, 2013.

[4] Y. Jiang, Q. Hu, and G. Ma. Adaptive backstepping fault-tolerant control for flexible spacecraft with unknown bounded disturbances and actuator failures. *ISA Transactions*, 49(1):57 – 69, 2010.

[5] M. V. De Wal and B. De Jager. A review of methods for input/output selection. *Automatica*, 37(4):487–510, 2001.

[6] K. Michail, A.C. Zolotas, and R.M Goodall. Optimised configuration of sensors for fault tolerant control of an electromagnetic suspension system. *International Journal of Systems Science*, 43(10):1785–1804, 2012.

[7] S. Skogestad and I. Postlethwaite. *Multivariable Feedback Control Analysis and Design*. John Wiley & Sons Ltd, 2^{nd} Edition, New York, 2005.

[8] D. C. McFarlane and K. Glover. A loop-shaping design procedure using $\mathcal{H}_\infty$ synthesis. *IEEE Transactions on Automatic Control*, 37(6):759–769, 1992.

[9] M. Blanke, R. Izadi-Zamanabadi, S. A. Bogh, and C. P. Lunau. Fault-tolerant control systems - a holistic view. *Control Engineering Practice*, 5(5):693–702, 1997.

[10] M. Blanke, M. Kinnaert, J. Lunze, and M. Staroswiecki. *Diagnosis and Fault-Tolerant Control*. Springer-Verlag New York, Inc., Secaucus, NJ, USA, 2003.

[11] I. Hwang, S. Kim, Y. Kim, and C.E. Seah. A survey of fault detection, isolation, and reconfiguration methods. *IEEE Transactions on Control Systems Technology*, 18(3):636–653, 2010.

[12] R. J. Patton. Fault-tolerant control: The 1997 situation. In *IFAC Symposium on Fault Detection Supervision and Safety for Technical Processes*, volume 3, pages 1029–1052, 1997.

[13] Y. Zhang and J. Jiang. Bibliographical review on reconfigurable fault-tolerant control systems. *Annual Reviews in Control*, 32(2):229–252, 12 2008.

[14] J. Dreo, P. Siarry, A. Petrowski, and E. Taillard. *Metaheuristics for Hard Optimization*. Springer-Verlg Berlin Heidelberg, New York, 2006.

[15] D. F. Jones, S. K. Mirrazavi, and M. Tamiz. Multi-objective meta-heuristics: An overview of the current state-of-the-art. *European Journal of Operational Research,*, 137(1):1–9, 2/16 2002.

[16] N. V. Dakev, J. F. Whidborne, A. J. Chipperfield, and P. J. Fleming. Evolutionary $\mathcal{H}_\infty$ design of an electromagnetic suspension control system for a maglev vehicle. *Proceedings of the Institution of Mechanical Engineers.Part I, Journal of Systems & Control Engineering*, 211(5):345–355, 1997.

[17] P. J. Fleming and R. C. Purshouse. Evolutionary algorithms in control systems engineering: A survey. *Control Engineering Practice*, 10(11):1223–1241, 2002.

[18] G. P. Liu, J. B. Yang, and J. F. Whidborne. *Multiobjective Optimisation and Control*. Research Studies Press, Baldock, UK, 2002.

[19] D. E. Goldberg. *Genetic algorithm in Search, Optimisation and Machine Learning*. Addison-Wesley Longman Publishing Co., Inc., Boston, MA, USA, 1989.

[20] A. Konak, D.W. Coit, and A.E. Smith. Multi-objective optimization using genetic algorithms: A tutorial. *Reliability Engineering and System Safety*, 91(9):992–1007, 2006.

[21] X. Zou, Y. Chen, M. Liu, and L. Kang. A new evolutionary algorithm for solving many-objective optimization problems. *IEEE Transactions on Systems, Man, and Cybernetics, Part B: Cybernetics*, 38(5):1402–1412, 2008.

[22] K. Deb, A. Pratap, S. Agarwal, and T. Meyarivan. A fast and elitist multiobjective genetic algorithm: NSGA-II. *IEEE Transactions on Evolutionary Computation*, 6(2):182–197, 2002.

[23] N. Meteopolis and S. Ulam. The monte carlo method. *Journal of the American Statistical Association*, 44(247):335–341, 1949.

[24] N. Metropolis. The beginning of the monte carlo method. *Los Alamos Science*, 15(584):125–130, 1987.

[25] M. H. Kalos and P. A. Whitlock. *Monte carlo methods.* Wiley-VCH, 2^{nd} Edition, 2008.

[26] H. Niederreiter. *Random number generation and quasi-Monte Carlo methods*, volume 63. Society for Industrial Mathematics, 1992.

[27] R. Tempo, G. Calafiore, and F. Dabbene. *Randomized Algorithms for Analysis and Control of Uncertain Systems.* Springer Verlag, 2004.

[28] H-W. Lee, K-C. Kim, and J. Lee. Review of maglev train technologies. *IEEE Transactions on Magnetics*, 42(7):1917–1925, 2006.

[29] R. M. Goodall. Generalised design models for EMS maglev. In *Proceedings of MAGLEV 2008 - The* 20^{th} *International Conference on Magnetically Levitated Systems and Linear Drives*, 2008.

[30] R. M. Goodall. Dynamics and control requirements for EMS maglev suspensions. In *Proceedings on international conference on Maglev*, pages 926–934, 2004.

[31] R. M. Goodall. The theory of electromagnetic levitation. *Physics in Technology*, 16(5):207–213, 1985.

[32] J. E. Paddison. Advanced control strategies for maglev suspension systems, 1995. PhD Dissertation, Loughborough Univeristy, School of Electronic, Electrical and Systems Engineering.

[33] R. M. Goodall. Dynamic characteristics in the design of maglev suspensions. *Proceedings of the Institution of Mechanical Engineers, Part F: Journal of Rail and Rapid Transit*, 208(1):33–41, 1994.

[34] K. Michail, A.C. Zolotas, and R.M. Goodall. Fallback options for airgap sensor fault of an electromagnetic suspension system. *Central European Journal of Engineering*, 3(2):206–220, 2013.

[35] C. A. C. Coello. Theoretical and numerical constraint-handling techniques used with evolutionary algorithms: A survey of the state of the art. *Computer Methods in Applied Mechanics and Engineering*, 191(11-12):1245–1287, 2002.

[36] K. Michail. Optimised configuration of sensing elements for control and fault tolerance applied to an electro-magnetic suspension system, 2009. PhD dissertation, Loughborough University, Scool of Electronic, Electrical and Systems Engineering. http://hdl.handle.net/2134/5806.

[37] B. Friedland. *Advanced Control System Design.* Prentice-Hall Inc., Upper Saddle River, NJ, USA, 1996.

[38] R. Isermann. Supervision, fault-detection and fault-diagnosis methods–an introduction. *Control Engineering Practice*, 5(5):639–652, 1997.